arXiv:1609.00304v1 [cond-mat.supr-con] 1 Sep 2016

Advanced surface characterization of $Ba(Fe_{0.92}Co_{0.08})_2As_2$ epitaxial thin films

D. Daghero[a,], P. Pecchio[a], F. Laviano[a], R.S. Gonnelli[a], F. Kurth[b], V. Grinenko[b], K. Iida[b]

[a] *Dipartimento di Scienza Applicata e Tecnologia, Politecnico di Torino, Corso Duca degli Abruzzi 24, 10129 Torino, Italy*
[b] *Leibniz-Institut für Festkörper-und Werkstoffforschung (IFW) Dresden, P.O.Box 270116, 01171 Dresden, Germany*

Abstract

We report on the systematic characterization of $Ba(Fe_{0.92}Co_{0.08})_2As_2$ epitaxial thin films on CaF_2 substrate in view of their possible use for superconducting electronic applications. By using different and complementary techniques we studied the morphological characteristics of the surface, the structural properties, the magnetic response, and the superconducting properties in terms of critical temperature, critical current, and energy gaps. Particular attention was paid to the homogeneity of the films and to the comparison of their superconducting properties with those of single crystals of the same compound.

Keywords: Iron-based superconductors, Thin films, Surface characterization, Point-contact spectroscopy, Transport properties, Magnetic properties

1. Introduction

The study on Fe-based superconductors is one of the most fruitful fields of present research in superconductivity. The rather high critical temperature of some of these compounds, their high critical fields and critical currents, the multiband electronic structure, the unprecedented sensitivity of the superconducting properties to the structural parameters, are of great interest

Email address: dario.daghero@polito.it (D. Daghero)

for both fundamental reasons and possible applications in transport and /or superconducting electronics [1]. Although the fundamental research is traditionally focused on single crystals, the synthesis of high-quality films is the indispensable step towards the fabrication of superconducting electronic devices that, in most cases, have Josephson junctions as their basic constituting element [2, 3]. Moreover, thin films are more suitable than single crystals for investigation of transport and optical properties, thanks to their dimensionality and the possibility to control their shape by lithography. Additionally, thin films are also important for fundamental research, since they allow exploring the effects of lattice deformation by strain/stress (hardly accessible in single crystals) on structural parameters, surface morphology, transport and fundamental properties.

The growth of epitaxial thin films of Co-doped $BaFe_2As_2$ on different substrates by using a simple pulsed-laser deposition (PLD) technique has been demonstrated since 2009 [4, 5, 6, 7]. A strong effect of the substrate on the critical temperature was observed, due to strain-induced modification of the ratio c/a of the cell parameters. Recently, the use of single-crystalline CaF_2 as a substrate has been shown to allow the growth of epitaxial films of $Ba(Fe_{1-x}Co_x)_2As_2$ with a record high critical temperature of nearly 28 K [8].

In this paper we present a systematic characterization of these films by means of various complementary techniques in order to test (and assess) their quality from the points of view of structure (epitaxy, texture), surface morphology (granularity, roughness), and superconducting properties via magnetic, transport and spectroscopic measurements. In particular, we compare the results of local and non-local techniques in order to check the homogeneity of the films; moreover, we compare the superconducting properties (critical temperature and gap amplitudes) to those of single crystals. The results provide thorough information on the features of these films, which is a basic step prior to their use for advanced fundamental studies and applications.

2. Thin film growth

The $Ba(Fe_{1-x}Co_x)_2As_2$ thin films, of thickness $t = 50$ nm, were deposited on (001) CaF_2 substrates by PLD [8] in ultra high vacuum (base pressure of 10^{-9} mbar) using a $Ba(Fe_{1-x}Co_x)_2As_2$ polycrystalline target with cobalt content $x = 0.08$. The high phase purity of the target was verified by means of powder X-ray diffraction (XRD) in Bragg-Brentano geometry [8, 9]; before the film deposition the target surface was cleaned by about 1000 laser pulses.

The CaF_2 substrate was cleaned in an ultrasonic bath by using acetone and isopropanol, and then subjected to an additional heat treatment at 700°C for 30 minutes. Because of the strain induced by the substrate, it is impossible to determine the Co content of the films by measuring the lattice parameters and comparing the results with single crystal data, as instead is commonly done in the case of the bulk material. The Co content was therefore measured directly by means of energy dispersive X-Ray (EDX) spectroscopy (with an EDX Oxford X-ACT spectrometer). Different spectra were taken on the same film, either over areas of a few square microns, or in single points. Because of the very small thickness of the films as compared to the depth probed by EDX, a large signal from the CaF_2 substrate was always observed. Nevertheless, the compositions determined from all these spectra turned out to be well consistent with one another. On averaging over all the spectra, the value $x = 0.074 \pm 0.017$ was obtained for the Co content, in very good agreement with the nominal value $x_{\rm nom} = 0.08$. The uncertainty $\delta x = 0.017$ is here equal to one half of the spread of x values obtained in single spectra.

3. Surface morphology

Figure 1a shows a reflection high-energy electron diffraction (RHEED) image of the CaF_2 substrate after cleaning and thermal treatment. Here the incident electron beam is parallel to the [110] direction of the CaF_2 substrate. It is clear from this figure that streaks and well distinct Kikuchi lines are observed, which indicate a smooth and single-crystal surface of CaF_2 substrate. A RHEED image of the Co-doped Ba-122 thin film grown on this substrate, taken just after the deposition, is shown instead in Figure 1b. The pattern in this case shows long streaks perpendicular to the shadow edge, and centered at positions on the Laue circles. This is typical for a multilevel surface, i.e. for a high number of grains with smooth terraces.

The morphology suggested by the RHEED is confirmed by direct imaging of the film surface by field-emission scanning electron microscopy (4248 Merlin ZEISS FESEM). Figure 2a shows a secondary-electron (SE) image taken over an area of about $1.8 \times 1.8\,\mu\mathrm{m}^2$. This image mainly carries morphological / topographical information; flat and smooth terraces, with parallel edges of about $100 - 150$ nm in size are clearly visible, which protrude from a pattern of well connected grains. This further indicates that Co-doped Ba-122 films grow in a terraced island mode. Figure 2b reports a greater-magnification (i.e. smaller-scale) image taken on a different region of the film surface,

and Figure 2c shows a backscattered-electron (BSE) image of the same area. A diagonal stripe-like pattern not related to the granular structure is very clearly seen in this picture (and also, though less clearly, in panel (b)); this pattern might be associated with correlated defects along the c-axis as also discussed in section 5.

Additional and complementary information about the surface morphology was collected by means of atomic-force microscopy (AFM) measurements. Figure 3a and b show two AFM images taken on the same region of the film, though on a different scale. The correspondence between color and height is shown by the vertical bar on the right side of each picture. The flat terraces with parallel edges already observed by FESEM are very clearly visible here; the additional information is that their top surface is flat but not perfectly horizontal. The distribution of heights calculated over the whole area shows a broad maximum at 5 nm, which indicates that the terraces protrude by (on average) 5 nm out of the underlying surface. The root mean square (RMS) roughness is 1.15 nm while the size of the terraces, determined by means of z-height profile cuts, ranges between 50 and 200 nm. Figure 3c shows the same image as in (b) but after a Prewitt gradient filtering, that allows highlighting the elevation of the terraces above the background.

4. Structural properties

A structural characterization of the films was carried out by means of X-ray diffraction spectroscopy. Figure 4a shows a $\theta - 2\theta$-scan in the Bragg-Brentano geometry, that demonstrates that the films grow free from impurities and secondary phases. Moreover, only the 00ℓ reflections from Co-doped Ba-122 and of the CaF_2 substrate are recorded, which proves that the film is c-axis oriented. Figure 4b reports ϕ-scans of the 112 reflection of Co-doped Ba-122 film (top curve). Strong and sharp peaks (average $\Delta\phi$ value of 0.73°) are observed every 90°, indicative of four-fold symmetry. The bottom curve in the same figure is a ϕ-scan of the 111 CaF_2 reflection, reported here for comparison and to confirm the epitaxial relation between the film and the substrate. Note that the CaF_2 substrate peaks appear 45° away from the Co-doped Ba-122 peaks. This clearly indicates that the Co-doped Ba-122 film is biaxially textured and its epitaxial relation with the substrate is (001)[110] Co-doped Ba-122 $\parallel$ (001)[100] CaF_2.

5. Transport and magnetic properties

Standard four-probe resistance measurements were performed in a ^{4}He cryostat to determine the transport critical temperature and the transition width. The measurements were conducted by using either the standard collinear configuration (with contacts along the diagonal of the 5 mm $\times$ 5 mm film) or the van der Pauw (vdP) configuration, with four contacts on the corners (see the left inset to Figure 5a). With respect to the collinear configuration, the vdP one allows probing a much larger region of the sample surface, and thus provides a well-representative measure of its average normal-state properties. In other words, if the measured resistivity is written as a weighted average over the entire sample surface, i.e. $\langle\rho\rangle = \int \rho(x,y)g(x,y)dxdy$ where $g(x,y)$ is a position-dependent weighting function, the vdP configuration allows maximizing the geometrical extension of the region (the so-called "sweet spot" [10, 11]) where the weighting function is maximum. In the case of a square sample with the contacts on its corners, as in our case, the van der Pauw resistance measurements probe an extended region of the film (of the order of some square millimeters) [11].

A typical result of a $R(T)$ measurement up to 250 K is shown in the right inset to Figure 5a (solid line). Here the current was flowing through the two top contacts and the voltage drop was measured across the bottom ones (see left inset). None of the curves measured in the films showed anomalies that could suggest the existence of macroscopic inhomogeneities either in the transition temperature or in the normal-state conductivity [12, 13]. In the normal state, the $R(T)$ curve displays a minimum around 75 K. A comparison with the resistivity curves of single crystals [14] shows that this shape is typical of the underdoped region, while in optimally-doped ($x = 0.061$) and overdoped crystals the $R(T)$ curve is monotonic. To clarify this point, the right inset to Figure 5a shows the resistance of the film compared to the resistivity of a single crystal with $x = 0.051$ (dashed line), both normalized to their values at 250 K. Further indication that our films lie in the slightly underdoped region of the phase diagram comes from the fact that in the films deposited on CaF_2 substrate the highest T_c is achieved for $x = 0.10$ [15]. It is clear therefore that the phase diagram of these films shows a superconducting dome which is shifted to higher doping (and also extends to higher temperature) with respect to that of single crystals. This fact has already been mentioned in our previous work [15]. The confirmation of the Co content of the films provided by EDX (see above) rules out a systematic

overestimation of the doping, so that the only factor responsible for the wider superconducting dome of films is the effect of the substrate [8].

Let us focus now on the superconducting transition. The resistance drops to 90% of its residual value at $T_c^{90} = 25.2$ K and to 10% at $T_c^{10} = 23.5$ K (see main panel of Figure 5a). The zero-resistance state is reached at $T_c^0 = 22.9$ K. Resistance measurements over a whole set of films with the same doping content (but from different batches) have given the average values $T_c^{10} = (23.85 \pm 0.35)$ K and $T_c^{90} = (25.4 \pm 0.2)$ K.

As mentioned above, the resistance measurement is definitely not a local one; and also the critical temperature is averaged over a large portion of the film. To check whether this measurement is representative of the *local* properties, we used a technique which is very seldom employed for that purpose, i.e. point-contact Andreev-reflection spectroscopy (PCARS) [16]. This consists in measuring the differential conductance of a point contact between a normal metal and the superconductor under study, as a function of the voltage applied across the contact itself. If the contact is small enough (i.e. smaller than the electronic mean free path) the dI/dV vs V curve shows a conductance enhancement due to Andreev reflection [17], that contains information about the amplitude and symmetry of the superconducting gap. Since the latter closes at the *local* critical temperature of the region where it is measured, PCARS can provide point-like measurements of the critical temperature, defined here as the temperature T_c^A at which the features associated to Andreev reflection disappear and the normal-state conductance is recovered.

To make the point contacts on the films [15], we used a thin Au wire ($\varnothing = 18\,\mu$m) kept in electrical and mechanical contact with the film surface in one single point, thanks to a small drop of Ag conducting paste. Although the diameter of the drop is rather large ($\varnothing \leq 100\,\mu$m), the effective contact occurs only here and there between the film surface and single Ag grains, naturally selecting the more conducting channels within a microscopic region. The spectrum of each point contact is thus actually an average (over a micrometric scale) of the signal of several nanometric contacts.

A comparison between the values of T_c^A we measured in different regions of a given film (hollow symbols) with the relevant R vs T curve (red filled symbols) is shown in the main panel of Figure 5. Here the abscissa of each hollow circle is the local T_c^A of a point contact; since each PCARS spectrum must be acquired at thermal equilibrium, the uncertainty on T_c^A comes from the temperature step between the first normal-state spectrum and the last

superconducting one. The ordinate of the points does not have a special meaning (it has been adjusted so that the points are superimposed to the $R(T)$ curve for ease of comparison). It is worth noting that all the values of the local T_c^A are close to T_c^{90} or lie between this temperature and T_c^{10}. The absence of T_c^A values that fall in the lower 10% of the resistive transition is an experimental evidence common to all the measured films. This fact certainly indicates that there is no significant heating in the contact region (i.e. the temperature of the contact is not higher than that of the bath), as instead would happen if the contacts were not in the proper spectroscopic regime.

The magnetic properties of the films were investigated in a Quantum Design SQUID magnetometer. The temperature dependence of the normalized magnetic moment $m(T)/m(1.8\text{K})$ is shown in Figure 5b (blue open symbols). In the experiment the film was cooled in zero magnetic field down to $T = 1.8$ K, then a magnetic field $H = 5$ Oe parallel to the ab plane of the film was applied, and the superconductor was heated up above T_c giving the zero-field-cooling (ZFC) curve in Figure 5b. After this, the film was again cooled down to $T = 1.8$ K in the presence of $H \parallel ab = 5$ Oe, and the field-cooling (FC) curve in Figure 5b was measured. The splitting between ZFC and FC curves corresponds to the temperature T_c^0 at which non-zero critical current appears in the film volume. In the case of the homogeneous superconducting state T_c^0 exactly corresponds to zero resistance. Usually, from the value of the diamagnetic signal at low temperatures (ZFC curve) it is possible to estimate the superconducting volume fraction in the sample. In our case the film thickness t is smaller than the magnetic penetration depth λ [1], therefore the value of ZFC signal does not correspond to the actual superconducting volume. However, the pronounced diamagnetic signal and the high transport critical currents (see below) indicate that a large volume fraction of the film is in the superconducting state at $T < T_c^0 \approx 23$ K.

To study the transport properties of the films in greater detail, we also measured the in-field critical current density J_c as a function of temperature and magnetic field. The measurements were carried out by using a standard 4-probe collinear configuration. A voltage criterion of $1\,\mu$V/cm was employed for evaluating J_c. The magnetic field H was applied in maximum Lorentz force configuration during all measurements. In Figure 6a, the field dependence of J_c is shown for both main crystallographic orientations of the magnetic field (i.e. $H \parallel c$ and $H \parallel ab$) in a temperature range between 10 and 22 K. In the low-field regime, J_c is very little dependent on the field direction (i.e. the critical current density is isotropic). This is even clearer

by looking at the angular dependence of J_c shown in Figure 6b. Here the angular dependence of the critical current is very weak (i.e. J_c is almost isotropic) up to magnetic field intensities of the order of 5 T. Actually J_c for $H \parallel c$ is slightly larger than that for $H \parallel ab$ below 3 T, which is unexpected from the electronic anisotropy of this system [18, 19]. Such an inverse correlation of J_c anisotropy strongly indicates the presence of defects along the c axis, that may be related to the irregular stripe-like pattern observed by FESEM in BSE mode.

6. Local energy gaps

The determination of the local gap values is not a standard surface characterization technique for films; however, the homogeneity of the gap amplitude over the surface is a useful indication if the films are meant to be used for electronic applications (especially in the long-term purpose of realizing circuits with multiple Josephson junctions, large-area SQUIDs and so on).

The values of the gaps were determined by means of PCARS in the same point contacts used for the measurement of the local T_c^A (see left inset to Figure 5a). Figure 7a shows two representative examples of normalized PCARS spectra measured at 4.2 K. In general, the normalization is obtained by dividing the raw spectrum ($dI(V)/dV$ vs V) of the normal-metal/superconductor (NS) junction by the same spectrum obtained when both the banks are in the normal state. Because of well-known effects associated to the large resistance of the films [20], however, the normal-state spectrum in our case is shifted downwards (see for example [15] and [21]) and cannot be used for this purpose. The normalization was therefore done with respect to the polynomial fit of the high-energy tails of the spectrum. This procedure gives rise to some uncertainty on the amplitude of the signal but does not affect the position of the structures associated to the energy gaps. In order to extract the gap values, the normalized spectra (open symbols) were fitted by using the standard two-band 2D BTK model [22, 23] with two isotropic gaps whose amplitudes will be called Δ_L (the larger) and Δ_S (the smaller). This is consistent with ARPES results in Co-doped Ba-122 [24] but also with the results of PCARS in single crystals of the same compound [25] at optimal doping. The result of the fit is shown as solid lines in Figure 7a. Since the model contains 7 parameters, the result is not univocal, i.e. there is a range of parameters that allows obtaining quantitatively acceptable fits within a certain interval of confidence. The gap values indicated in the labels are actually the midpoints

of the range of acceptable Δ_S and Δ_L values, and the uncertainty expresses the half-width of that range. Figure 7b reports the values of the gaps obtained in different point contacts. The values are rather well compatible with one another; in particular, a good homogeneity of the small gap is observed, while the large gap shows greater spread: it varies within a range of about 3 meV including the error bars (this spread is however not unusual in Fe-based compounds [16]). Note that, as shown elsewhere [15], the gap amplitudes shows no dependence on the contact resistance, that here varies by over one order of magnitude. The values of the gaps obtained in these films may be compared to those obtained in single crystals. In general, this comparison can tell whether the superconducting properties of the bulk are weakened in thin films. Here, because of the strong effect of the substrate, thin films are structurally different from the bulk material so that this comparison must be taken more cautiously. Anyway, just for the sake of discussion, the gap values measured in *c*-axis contacts in single crystals with critical temperature (measured by transport) $T_c^{\rm onset} = 24.5$ K turned out to be $\Delta_S = 4.1 \pm 0.4$ meV and $\Delta_L = 9.2 \pm 1.0$ meV [25]. These ranges are indicated in Figure 7b by dashed bands. It is clear that the values of Δ_S and Δ_L obtained in crystals lie well within the range of measured amplitudes in films, although in the latter case the spread is larger for both the small and the large gap. It is also true, however, that single crystals were much smaller than the films (the top surface area was at most $1 \times 1\,\mathrm{mm}^2$) and that an extensive study of the spatial homogeneity of the gaps in these samples was not performed.

7. Conclusions

Co-doped Ba-122 thin films of thickness $t = 50$ nm were prepared by pulsed laser deposition on (001)CaF_2 single crystalline substrates and morphologically, structurally and electro-magnetically characterized by means of various experimental techniques. RHEED, FESEM and AFM analyses show that the films grow in a terraced island mode, with flat rectangular terraces of about 100 nm in size protruding by about 5 nm out of a background of well-connected grains. The surface is very smooth and homogeneous, with a small RMS roughness of 1.15 nm. As demonstrated by $\theta - 2\theta$ XRD scans, the films are free from impurities and secondary phases, and are *c*-axis oriented; ϕ scans also show that they are highly biaxial textured, with the $Ba(Fe_{1-x}Co_x)_2As_2$ cell rotated by 45° with respect to that of the CaF_2 substrate. The actual cobalt content, measured by EDX, is $x = 0.074 \pm 0.017$, in

good agreement with the nominal one $x_{\mathrm{nom}} = 0.08$. Nevertheless, these films are slightly underdoped (indeed, the maximum T_{c} is achieved for $x = 0.10$) as also witnessed by the minimum in their $R(T)$ curve. The discrepancy with the case of single crystals (where optimal doping occurs at $x = 0.061$ [14]) is thus likely to arise from the strong compressive strain (and the consequent enhancement of the c/a ratio) induced by the CaF_2 substrate on Co-doped Ba-122 [8]. The critical temperature determined by electric transport measurements is indeed by almost 2 K higher than that of single crystals with the same cobalt content. The local surface critical temperature $T_{\mathrm{c}}^{\mathrm{A}}$ determined by point-contact spectroscopy in different regions of a given film turns out to be in perfect agreement with the resistive transition; moreover, evidence for bulk superconductivity is given by magnetization measurements, which also show the correspondence between the onset of a diamagnetic signal and the achievement of the zero-resistance state. The superconducting gaps (in particular the smaller one, Δ_{S}, which generally plays a major role in tunneling and presumably also in Josephson effect [3]) are rather homogeneous over the surface on a millimetric scale, and their amplitudes are well compatible with those measured in single crystals of the same compound. All these features are fundamental in view of applications in superconducting electronics. Finally, the rather high critical current density and its small anisotropy (promising for magneto-transport applications) suggest the presence of defects along the c axis, acting as pinning centers for $H \parallel c$, as also shown by FESEM BSE imaging. In conclusion, our Co-doped Ba-122 thin films show robust and homogeneous superconducting properties – in some respect analogous to those of single crystals – which are very promising for fundamental studies and superconducting applications, although some focused optimization of these properties can be envisaged in view of their use for specific purposes.

8. Acknowledgements

The authors wish to thank Mauro Raimondo for FESEM and EDX measurements. This work was done under the Collaborative EU-Japan Project "IRON SEA" (NMP3-SL-2011-283141).

References

[1] D. Jonhston, The puzzle of high temperature superconductivity in layered iron pnictides and chalcogenides, Advances in Physics 59 (2010)

803.

[2] A. L. Kadin, Introduction to Superconducting Circuits, Wiley-Interscience, 1999.

[3] P. Seidel, Josephson effects in iron based superconductors, Supercond. Sci. Technol. 24 (2011) 043001.

[4] T. Katase, H. Hiramatsu, H. Yanagi, T. Kamiya, M. Hirano, H. Hosono, Atomically-flat, chemically-stable, superconducting epitaxial thin film of iron-based superconductor, cobalt-doped $BaFe_2As_2$, Solid State Comunications 149 (2009) 2121–2124.

[5] K. Iida, J. Hänisch, R. Hühne, F. Kurth, M. Kidszun, S. Haindl, J. Werner, L. Schultz, B. Holzapfel, Strong T_C dependence for strained epitaxial $Ba(Fe_{1-x}Co_x)_2As_2$ thin films, Appl. Phys. Lett 95 (2009) 192501.

[6] S. Lee, J. Jiang, Y. Zhang, C. Bark, C. Weiss, J. D.and Tarantini, C. T. Nelson, H. Jang, C. M. Folkman, S. H. Baek, A. Polyanskii, D. Abraimov, A. Yamamoto, J. Park, X. Q. Pan, E. E. Hellstrom, D. C. Larbalestier, C. B. Eom, Template engineering of Co-doped $BaFe_2As_2$ single-crystal thin films, Nature Mater. 9 (2010) 397.

[7] J. Engelmann, V. Grinenko, P. Chekhonin, W. Skrotzki, D. Efremov, S. Oswald, K. Iida, R. Hühne, J. Hänisch, M. Hoffmann, F. Kurth, L. Schultz, B. Holzapfel, Strain induced superconductivity in the parent compound $BaFe_2As_2$, Nature Communications 4 (2013) 2877.

[8] F. Kurth, E. Reich, J. Hänisch, A. Ichinose, I. Tsukada, R. Hühne, S. Trommler, J. Engelmann, L. Schultz, B. Holzapfel, K. Iida, Versatile fluoride substrates for Fe-based superconducting thin films, Appl. Phys. Lett. 102 (2013) 142601.

[9] F. Kurth, K. Iida, S. Trommler, J. Hänisch, K. Nenkov, J. Engelmann, S. Oswald, J. Werner, L. Schultz, B. Holzapfel, S. Haindl, Electronic phase diagram of disordered Co doped $BaFe_2As_2$, Supercond. Sci. Technol. 26 (2013) 025014.

[10] D. Koon, C. J. Knickerbocker, Effects of macroscopic inhomogeneities on resistive and Hall measurements on crosses, cloverleafs, and bars, Rev. Sci. Instrum. 67 (1996) 4282.

[11] D. Koon, W. K. Chan, Direct measurement of the resistivity weighting function, Rev. Sci. Instrum. 69 (1998) 4218.

[12] R. Vaglio, C. Attanasio, L. Maritato, A. Ruosi, Explanation of the resistance-peak anomaly in nonhomogeneous superconductors, Phys. Rev. B 47 (1993) 15302.

[13] J. Mosqueira, A. Pomar, A. Díaz, J. A. Veira, F. Vidal, Resistivity anomalies above the superconducting transition in $Y_1Ba_2Cu_3O_{7-\delta}$ crystals and non-uniformly distributed critical-temperature inhomogeneities, Physica C 34 (1994) 225.

[14] J.-H. Chu, J. G. Analytis, C. Kucharczyk, I. R. Fisher, Determination of the phase diagram of the electron-doped superconductor $Ba(Fe_{1-x}Co_x)_2As_2$, Phys. Rev. B 79 (2009) 014506.

[15] P. Pecchio, D. Daghero, G. A. Ummarino, R. S. Gonnelli, F. Kurth, B. Holzapfel, K. Iida, Doping and critical-temperature dependence of the energy gaps in $Ba(Fe_{1-x}Co_x)_2As_2$ thin films, Phys. Rev. B 88 (2013) 174506.

[16] D. Daghero, R. Gonnelli, Probing multiband superconductivity by point-contact spectroscopy, Supercond. Sci. Technol. 23 (2010) 043001.

[17] A. Andreev, Thermal conductivity of the intermediate state of superconductors, Zh. Eksp. Teor. Fiz. 46 (1964) 1823, engl. Transl. Sov. Phys.-JETP **19**, 1228 (1974).

[18] K. Iida, T. Hänisch, T. Thersleff, F. Kurth, M. Kidszun, S. Haindl, R. Hühne, L. Schultz, B. Holzapfel, Scaling behavior of the critical current in clean epitaxial $Ba(Fe_{1-x}Co_x)_2As_2$ thin films, Phys. Rev. B 81 (2010) 100507(R).

[19] M. Putti, I. Pallecchi, E. Bellingeri, M. R. Cimberle, M. Tropeano, C. Ferdeghini, A. Palenzona, C. Tarantini, A. Yamamoto, J. Jiang, J. Jaroszynski, F. Kametani, D. Abraimov, A. Polyanskii, J. D. Weiss, E. E. Hellstrom, A. Gurevich, D. C. Larbalestier, R. Jin, B. C. Sales,

A. S. Sefat, M. A. McGuire, D. Mandrus, P. Cheng, Y. Jia, H. H. Wen, S. Lee, C. B. Eom, New Fe-based superconductors: properties relevant for applications, Supercond. Sci. Technol. 23 (2010) 034003.

[20] T. Y. Chen, S. X. Huang, C. L. Chien, Pronounced effects of additional resistance in Andreev reflection spectroscopy, Phys. Rev. B 81 (2010) 214444.

[21] S. Döring, S. Schmidt, S. Gottwals, , S. Schmidl, V. Tympel, I. Mönch, F. Kurth, K. Iida, B. Holzapfel, P. Seidel, Influence of the spreading resistance on the conductance spectrum of planar hybrid thin film SNS' junctions based on iron pnictides, unpublished, arXiv:1309.1641 (Sep 2013).

[22] G. E. Blonder, M. Tinkham, T. M. Klapwijk, Transition from metallic to tunneling regimes in superconducting microconstrictions: Excess current, charge imbalance, and supercurrent, Phys. Rev. B 25 (1982) 4515.

[23] S. Kashiwaya, Y. Tanaka, Tunnelling effects on surface bound states in unconventional superconductors, Rep. Prog. Phys. 63 (2000) 16411724.

[24] K. Terashima, Y. Sekiba, J. H. Bowen, K. Nakayama, T. Kawahara, T. Sato, P. Richard, Y.-M. Xu, L. J. Li, G. H. Cao, Z.-A. Xu, H. Ding, T. Takahashi, Fermi surface nesting induced strong pairing in iron-based superconductors, Proc. Natl. Acad. Sci (USA) 106 (2009) 7330.

[25] M. Tortello, D. Daghero, G. A. Ummarino, V. A. Stepanov, J. Jiang, J. D. Weiss, E. E. Hellstrom, R. S. Gonnelli, Multigap Superconductivity and Strong Electron-Boson Coupling in Fe-Based Superconductors: A Point-Contact Andreev-Reflection Study of $Ba(Fe_{1-x}Co_x)_2As_2$ Single Crystals, Phys. Rev. Lett. 105 (2010) 237002.

9. Figure Captions

Figure 1
RHEED images of (a) the CaF_2 substrate and (b) the 8 % Co-doped Ba-122 thin film. In the latter case, the picture was acquired after the deposition at room temperature. As discussed in the text, the basal plane of Co-doped Ba-122 is rotated by 45° with respect to the substrate. Hence the electron beam is here parallel to the [100] direction of the Co-doped Ba-122.

Figure 2
FESEM images of the surface of a 8% Co-doped Ba-122 thin film deposited on CaF_2 substrate. (a,b) Two representative secondary-electron (SE) images with different magnifications (the scale is indicated in the labels). Clear, regular, flat terraces of rectangular shape (side length approximately 100 nm) are seen that protrude from an array of well-connected grains. (c) Backscattered-electron (BSE) image of the same area as in (b), that shows a diagonal stripe-like pattern not related to the granular structure, and possibly indicating the existence of correlated defects parallel to the c axis (i.e. perpendicular to the plane of the figure).

Figure 3
Examples of AFM measurements on the surface of a Co-doped Ba-122 thin film. (a) AFM image over an area of $3.75\,\mu\mathrm{m} \times 3.75\,\mu\mathrm{m}$, exhibiting a clear pattern of flat, rectangular terraces of about 100 nm in size. A comparison with the FESEM image of Figure 2a (taken on a similar scale) shows that the morphological information provided by FESEM and AFM is perfectly consistent; note that the latter does not show the stripe-like pattern seen in Figure 2c. (b) AFM image over a smaller area of $2\,\mu\mathrm{m} \times 2\,\mu\mathrm{m}$ and thus with a greater magnification. (c) The same image as in (b) but after application of a Prewitt horizontal gradient filter so as to highlight the elevation of the terraces above the background of well-connected grains.

Figure 4
Summary of structural characterization by X-ray diffraction. (a) $\theta - 2\theta$ scans in the Bragg-Brentano geometry with Co-Kα radiation; (b) ϕ-scans in a texture goniometer with Cu-Kα radiation for the 112 reflection of Co-doped Ba-122 and the 111 reflection of CaF_2.

Figure 5
Transport and magnetic measurements on a Co-doped Ba-122 thin film. (a)

The local critical temperature determined by PCARS (hollow symbols) compared to the resistive transition of the same film (red filled symbols). Left inset: a drawing of the film indicating the contacts used for the resistance measurement (red dots) and the regions where the point contacts were made (white dots). Right inset: the normalized resistance $R(T)/R(250\text{K})$ compared to that of slightly underdoped single crystals (from [14]). (b) Temperature dependence of the normalized magnetic moment $m(T)/m(1.8\text{K})$ of the film (blue open symbols) compared to the resistive transition of the same film (red filled symbols).

Figure 6

Summary of critical current measurements on a Co-doped Ba-122 thin film. (a) Field dependence (up to 9 T) of the critical current density J_c for $H \parallel c$ (open symbols) and $H \parallel ab$ (solid symbols) at various temperatures. (b) Angular dependence of J_c measured at $T = 14$ K and in the presence of magnetic fields of different intensity, from 1 T to 9 T.

Figure 7

Examples of PCARS results on a Co-doped Ba-122 thin film. (a) Two examples of normalized PCARS spectra measured in different points of the same 8% Co-doped film (symbols) with the relevant 2D BTK fit (lines). The values of the gap amplitudes Δ_L and Δ_S are indicated in the labels. (b) Summary of gap values obtained in different spectra in the same film (squares). The horizontal dashed bands represent the range of gap values found in single crystals with the same doping content.

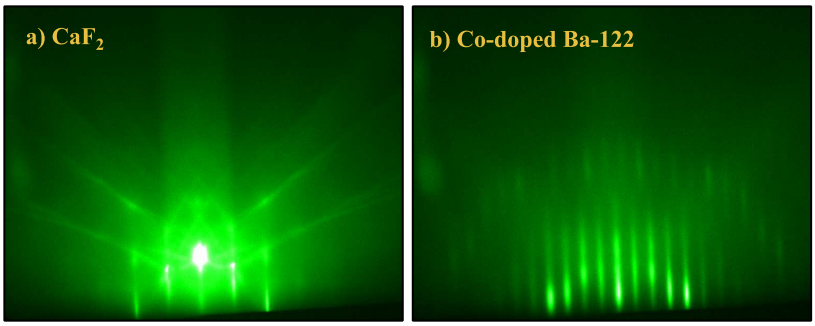


Figure 1:

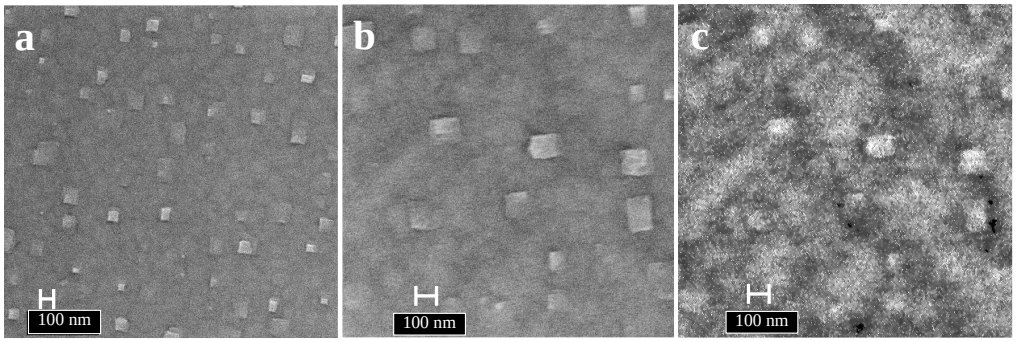


Figure 2:

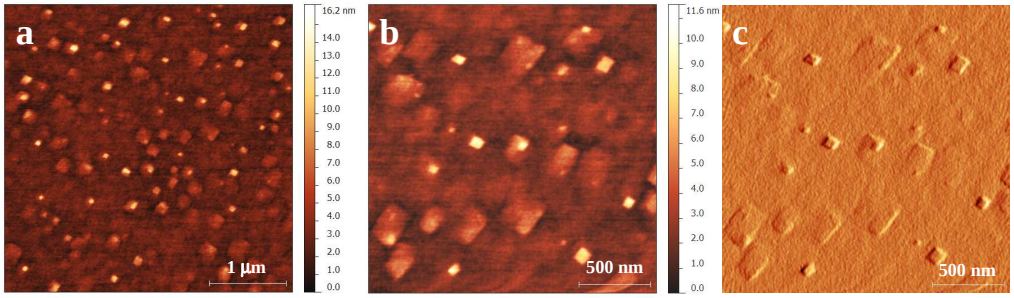


Figure 3:

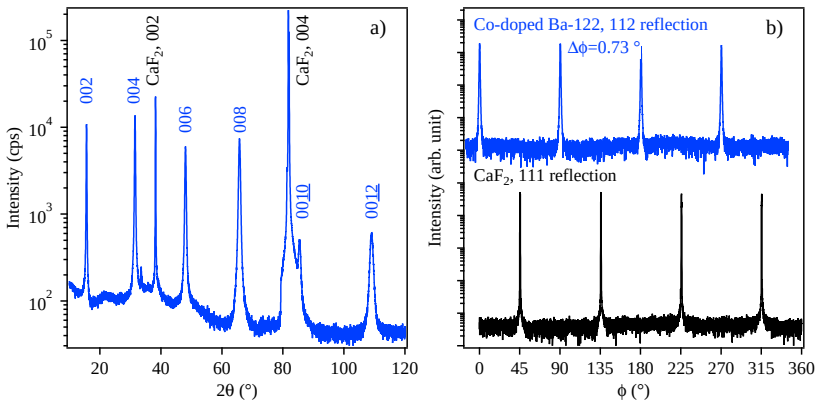


Figure 4:

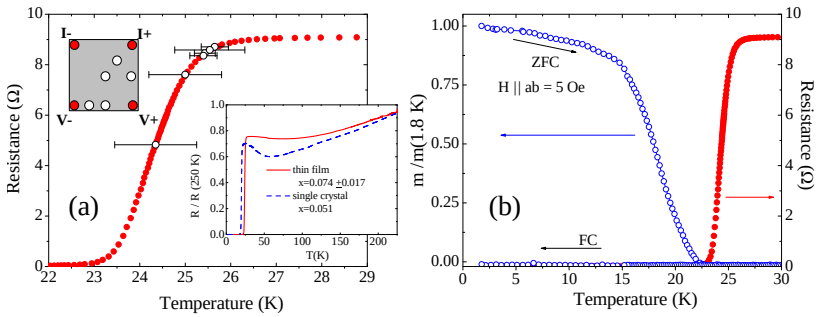


Figure 5:

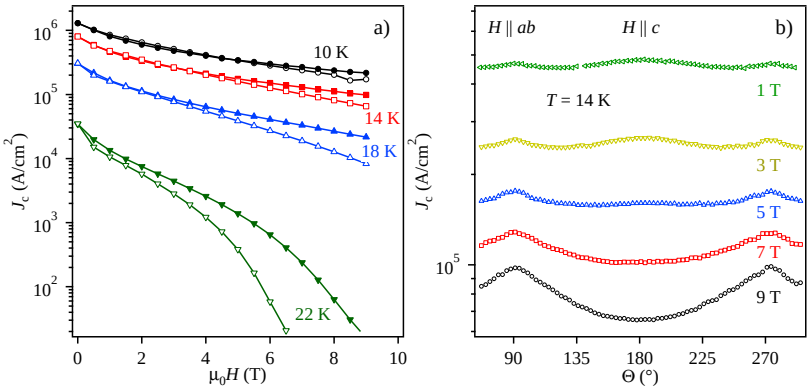


Figure 6:

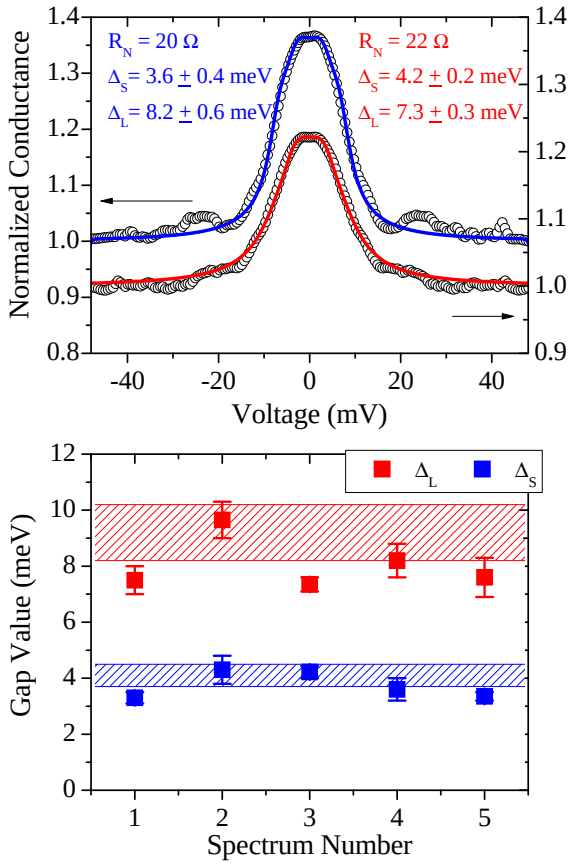

R_N = 20 Ω
Δ_S = 3.6 ± 0.4 meV
Δ_L = 8.2 ± 0.6 meV
R_N = 22 Ω
Δ_S = 4.2 ± 0.2 meV
Δ_L = 7.3 ± 0.3 meV
Normalized Conductance
Voltage (mV)
Δ_L
Δ_S
Gap Value (meV)
Spectrum Number

Figure 7: